Integrative and Comparative Biology

Integrative and Comparative Biology, volume 59, number 6, pp. 1597–1608
doi:10.1093/icb/icz144

Society for Integrative and Comparative Biology

SYMPOSIUM

Thermodynamics of the Bladderwort Feeding Strike—Suction Power from Elastic Energy Storage

Otto Berg,[*] Krizma Singh,[†] Maxwell R. Hall,[†] M. Janneke Schwaner,[‡] and Ulrike K. Müller[1,†]

[*]Department of Chemistry, California State University Fresno, Fresno, CA 93740, USA; [†]Department of Biology, California State University Fresno, Fresno, CA 93740, USA; [‡]Department of Biological Sciences, University of Idaho, Moscow, ID 83844, USA

From the symposium "Playing with Power: Mechanisms of Energy Flow in Organismal Movement" presented at the annual meeting of the Society for Integrative and Comparative Biology, January 3–7, 2019 at Tampa, Florida.

[1]E-mail: umuller@csufresno.edu

Synopsis The carnivorous plant bladderwort exemplifies the use of accumulated elastic energy to power motion: respiration-driven pumps slowly load the walls of its suction traps with elastic energy (~1 h). During a feeding strike, this energy is released suddenly to accelerate water (~1 ms). However, due to the traps' small size and concomitant low Reynolds number, a significant fraction of the stored energy may be dissipated as viscous friction. Such losses and the mechanical reversibility of Stokes flow are thought to degrade the feeding success of other suction feeders in this size range, such as larval fish. In contrast, triggered bladderwort traps are generally successful. By mapping the energy budget of a bladderwort feeding strike, we illustrate how this smallest of suction feeders can perform like an adult fish.

The elastic energy stored in loaded bladders—pressure–volume work performed during the loading process—is in the range of 1 μJ, as measured via the volume evacuated during loading, and literature values of internal pressure. We determined the kinetic energy present in the fluid during suction events from flow fields obtained by Particle Image Velocimetry. Such observations are confounded by the difficult-to-resolve timescale and internal flows, so we obtained independent estimates from mathematical and mechanical models. At the beginning of a feeding strike, we find that 0.5 mW of power is delivered by the elastic recoil mechanism, and the same amount appears as kinetic energy in the flow field. A power deficit would represent viscous dissipation heating the fluid by friction. Approximate solution of the Navier–Stokes equations for an idealized bladderwort strike suggests that less than 20% of power is lost to friction on the timescale relevant to prey capture. This discrepancy would indeed be difficult to detect experimentally. However, even this upper limit is small in comparison with the 60% losses calculated for fish larvae of similar size, the suction of which is assumed to be muscle powered (and for which elastic energy accumulation has not been demonstrated). Our estimates of elastic energy storage and frictional losses during suction events support the hypothesis that small suction feeders convert a large proportion of the elastic energy stored in the trap walls into kinetic energy of the inspired water, with little energy thermalized due to friction.

Introduction

This study aims to explore a particular prey capture behavior—suction feeding—and how it is powered. We do so by focusing on an organism—the carnivorous plant bladderwort (genus *Utricularia*)—whose suction feeding process is particularly amenable to such a power analysis, in contrast to animal suction feeders, whose feedings strikes are a complex interplay of muscle-driven suction (sometimes augmented by elastic energy release), deformation of the mouth (including jaw protrusion), and whole-body propulsion (Wainwright et al. 2001; Higham et al. 2006a; van Wassenbergh et al. 2008; Holzman et al. 2008; Camp et al. 2015). For this study, we combine (largely unpublished) experimental and

Advance Access publication August 13, 2019

modeling data on bladderwort suction strikes to describe the energy flow of a suction event (Berg et al. 2020).

Prey capture is a behavior that often requires the predator to generate extreme accelerations, be it of the predator's entire body or just the body part that constitutes the trapping mechanism. Many of biology's most extreme acceleration performances occur during prey capture by ambush predators, such as claw strikes of mantis shrimps (Patek et al. 2004), and ballistic tongue protection of chameleons (Wainwright et al. 1991) and lungless salamanders (Deban et al. 1997). These extreme-performance ambush predators use elastic mechanisms to generate the high powers required for such capture behaviors to accelerate specialized body parts (de Groot and van Leeuwen 2004; Deban et al. 2007; Zack et al. 2009). Aquatic predators can use a capture mechanism that combines this tactic of accelerating the predator toward the prey with a tactic that accelerates the prey toward the predator: many fish combine ram feeding (i.e., acceleration of the entire predator toward the prey) and jaw protrusion (accelerate a body part toward the prey) with suction feeding (accelerate the prey; Wainwright et al. 2001). Fish must generate considerable power during suction events, ranging from 0.2 to 12 kW/kg jaw muscle (Aerts et al. 1987; van Wassenbergh et al. 2008; Carroll and Wainwright 2009) for fish ranging in size from 10 to 190 g.

Suction feeding is common among aquatic vertebrates and is considered one of the main innovations in vertebrate evolution. Suction feeding is used across a wide size range, from first-feeding tadpoles and fish larvae (gape sizes smaller than 0.2 mm) to aquatic salamanders and adult fish (gape sizes in excess of 40 mm; Deban and Olsen 2002; van Wassenbergh et al. 2005; Stinson and Deban 2017). Whereas biological and solid-mechanical scaling laws might favor small suction feeders (Ilton et al. 2018; Olberding and Deban 2018), hydrodynamic scaling laws favor suction feeders above a critical size to avoid the drop in suction flow speed and energetic efficiency due to viscous friction (Drost et al. 1988; Yaniv et al. 2014). Computational models predict that suction feeders the size of larval fish could lose 60% of flow energy to friction (Drost et al. 1988). In the extreme case of a creeping flow regime (Poiseuille flow), flow speed is proportional to the fourth power of pipe diameter, causing narrow pipes to experience extremely slow flows. These mathematical predictions are supported by experimental observations on larval fish, whose suction performance improves markedly as their growing size allows them to move further away from the viscous flow regime (China and Holzman 2014).

Suction feeders generate quickly accelerating, high-speed suction flows with strong spatial pressure gradients to entrain and capture prey. Capture success correlates with rate of volume change and flow speed (van Wassenbergh et al. 2006; Holzman et al. 2012), and the power required for suction feeding correlates with the same factors (Camp et al. 2015). Estimates of required powers range from 10 to 4000 W/kg jaw muscle (peak power: 10–4000 W/kg, van Wassenbergh et al. 2005; average power: 195 W/kg, Aerts et al. 1987; 300 ± 75 W/kg, Carroll and Wainwright 2009), values high enough that some fish cannot rely exclusively on their jaw muscles to power suction feeding. Fish can power suction events directly using axial muscles (Camp et al. 2015) and indirectly via elastic energy storage and release (van Wassenbergh et al. 2008; van Wassenbergh and Aerts 2009a). In contrast to animal suction feeders, plant suction feeders (underwater traps of the carnivorous genus *Utricularia*) cannot use muscle power and instead rely exclusively on releasing stored elastic energy to power suction feeding events.

The carnivorous plant genus *Utricularia* (bladderworts) has many aquatic species with active underwater traps (Westermeier et al. 2017). These traps are highly modified leaflets (Rutishauser 2016) in the shape of a hollow bladder (diameter 0.5–8 mm; Poppinga et al. 2016). Bladderwort traps can be grouped into several types based mainly on the morphology of the entrance region (Westermeier et al. 2017). Within the aquatic bladderwort species, the best described trap type is the *U. vulgaris* type, which has a short channel, and a trap door that is approximately at right angles to the channel and opens with a snap-buckling mechanism (Vincent et al. 2011; Westermeier et al. 2017; Fig. 1). Traps are set by osmotically pumping water out of the lumen of the sealed bladder, which causes the bladder walls to become elastically loaded as sub-ambient pressure builds in the trap (Sasago and Sibaoka 1985a, 1985b; Joyeux et al. 2011; Singh et al. 2011). Traps snap when prey touches the trigger hairs on the trap door, causing the door to snap-buckle inward and the prey to be sucked into the trap (Joyeux et al. 2011; Vincent and Marmottant 2011).

Bladderwort suction traps are substantively different from a typical suction-feeding fish, such as largemouth bass (Carroll and Wainwright 2006; Higham et al. 2006b). Bladderworts rely entirely on stored elastic energy to power suction feeding, whereas largemouth bass use muscles (Camp et al. 2015).

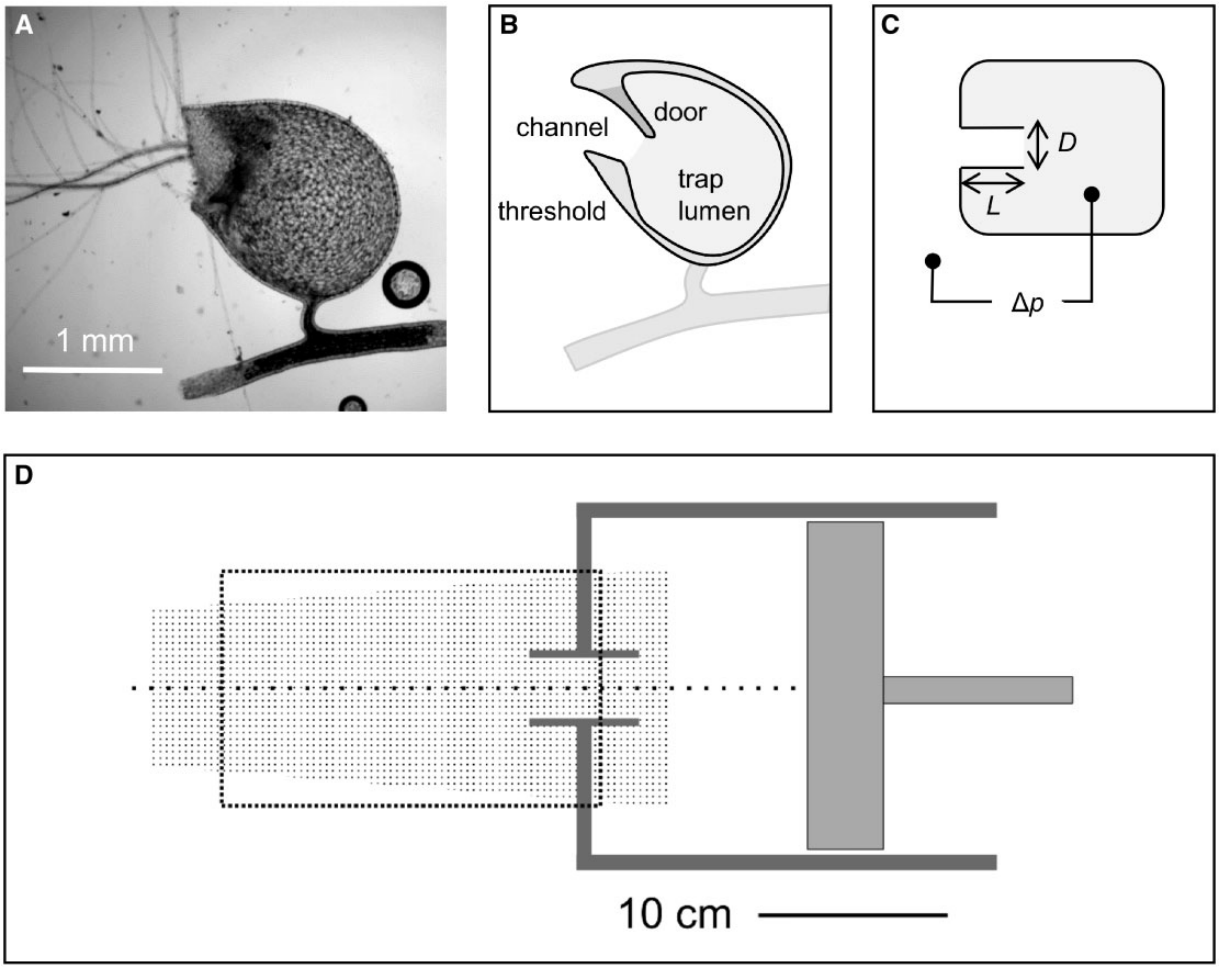

Fig. 1 Representation of a bladderwort trap as a mathematical and a mechanical model. (**A**) Side view of a loaded trap of *U. gibba* (door closed). (**B**) Sketch of a trap during suction (door open), indicating the channel (formed by the trap's door and threshold) through which water enters the trap lumen. (**C**) Mathematical model of a trap, modeling suction flows driven by a pressure difference Δp through a channel of diameter D (= "gape") and length L. (**D**) Mechanical model of a trap, modeling suction flows through a cylindrical channel driven by displacing a plunger (light gray) into a rectangular Perspex box (dark gray); indicated are the field of view of the camera (stippled outline) and the flow area illuminated by the laser (stippled area).

This difference in input power leads to important differences in the timing of energy flows. Bladderworts decouple the generation of suction pressure from the generation of suction flow: the traps generate a sub-ambient pressure before the trap door opens and suction commences (Singh et al. 2011; Fig. 2). In contrast, largemouth bass builds suction pressure while their mouth is opening (Carroll and Wainwright 2006; Higham et al. 2006b). We use conservation of energy to observe the energy flow during the loading and firing of a bladderwort trap (Fig. 2): during the loading phase, bladderworts convert chemical energy into elastic energy stored in the trap walls and into thermal energy (Sasago and Sibaoka 1985a, 1985b); during the firing phase, bladderworts convert elastic energy stored in the walls into kinetic energy that accelerates water into the trap and into thermal energy (mainly due to viscous friction); after the firing phase, all kinetic energy in the water is ultimately thermalized.

In this study, we explore the energy demands of a bladderwort suction cycle. Because the different forms of energy are separated in space (i.e., trap walls vs. water) and time (i.e., loading vs. firing of the trap), we can quantify separate steps of the energy transduction cascade of a suction cycle: the loading phase and the firing phase. The elastic potential energy stored in the trap walls during the loading phase is equal to the mechanical work of loading, specifically the volume of water pumped

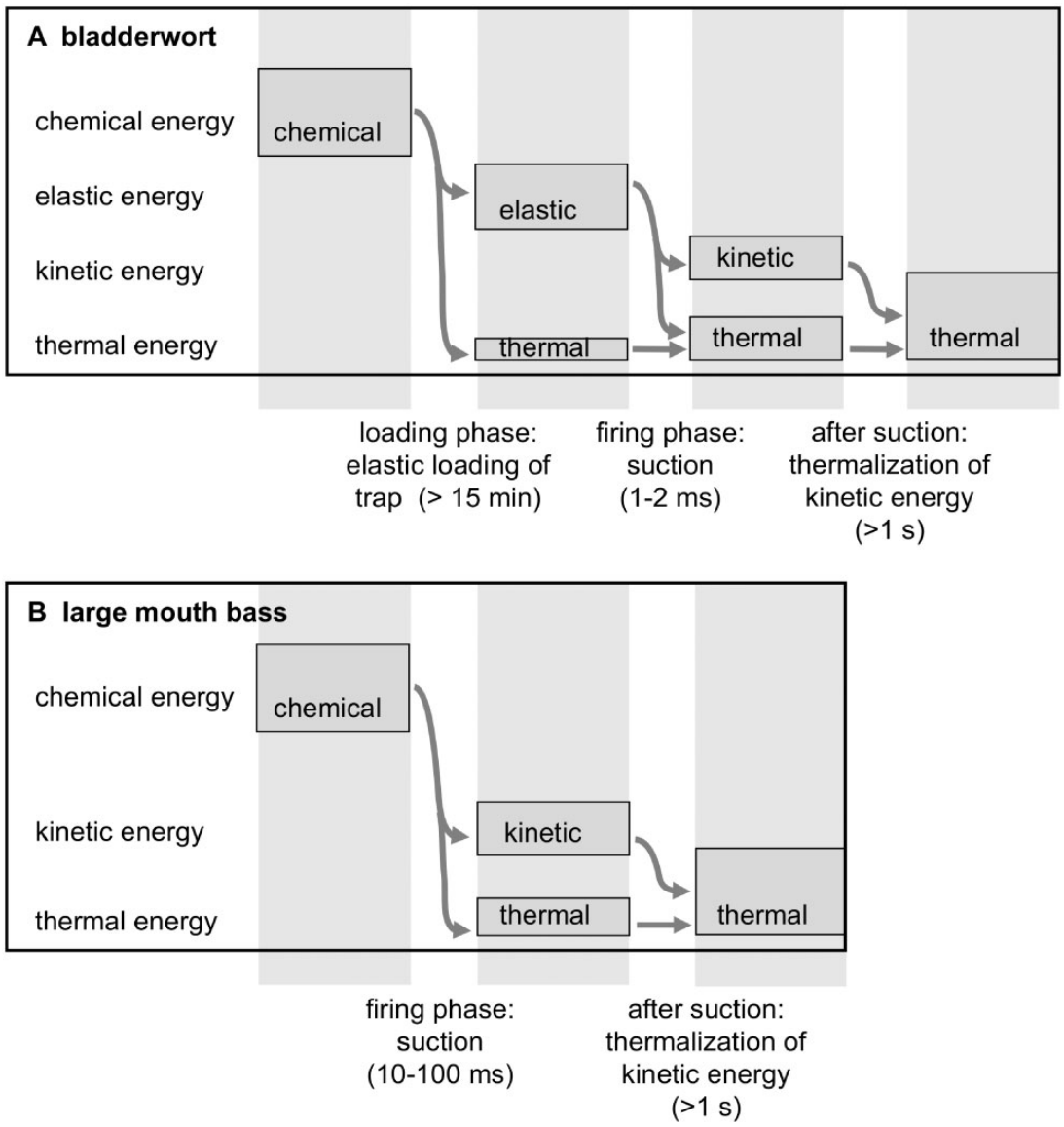

Fig. 2 Energy flow through plant and animal suction feeders. (**A**) Bladderworts convert chemical into elastic and thermal energy during the loading phase, then convert elastic energy into kinetic and thermal energy during the firing phase. (**B**) Largemouth bass converts chemical energy into kinetic energy during the firing phase. All energy is ultimately thermalized in both organisms.

out of the bladder lumen, against the pressure difference created by elastic deformation (Fig. 1). The power delivered during a subsequent firing phase can be calculated from the same pressure difference and the measured fluid flow rate. At a given instant, the portion of this power appearing as kinetic energy of the accelerating fluid can be determined from the time dependence of its vectorial flow field. Power missing from this macroscopic balance must be dissipated by friction.

The challenges of flow visualization on the scale of a bladderwort trap are overcome by means of a dynamically scaled mechanical model (Koehl 2003). At the key moment of the highest acceleration, we find that the elastic power (rate at which elastic energy is released from the trap walls) and kinematic power (rate at which kinetic energy appears in the water) are in satisfactory agreement. This good agreement suggests that viscous losses during this energy conversion are relatively small.

Methods

Plant material

We cultivated *Utricularia gibba* (stock obtained from the California Carnivores, Sebastopol, CA) in the departmental green house (natural lighting conditions; temperature controlled), following the

handling and care instructions outlined by Peter D'amato (2013).

Volume measurements

To estimate the energy expended during the loading of the trap, we determined the volume of water inspired into the bladder lumen during a suction event. We excised mature, loaded bladders from mature nodes (traps containing no debris, prey, or air bubbles). Bladders were excised using micro dissecting tweezers (Roboz, Gaithersburg, MD), blotted off by placing them on tissue paper, weighed on an analytical microbalance (Mettler Toledo MT5, Columbus, OH), then artificially triggered under water by touching the trigger hairs with a probe, then weighed again.

Visualization and analysis of fluid flow

To estimate the kinetic energy appearing in the fluid during the unloading of the trap, we developed a mechanical scaled model. This model was validated by comparing the flows generated by bladderwort traps with flows observed in the mechanical model.

Experiments using bladderwort traps

To visualize the suction flows generated by bladderwort traps, individual traps were selected from plant nodes with all mature traps. A selected trap was removed from the plant at the stolon and attached to a fine wire using cyanoacrylate glue (Loctite Super Glue Gel), then placed in a glass cuvette (Starna, dimensions: $5 \times 5 \times 15$ mm^3) filled with room-temperature water. Traps were mounted at least two gape diameters from cuvette walls to avoid wall effects.

Manually triggered suction events were recorded with a Phantom V12.1 high speed camera (Vision Research) at 50,000 frames/s (320×280 pixels^2). The macro imaging system consisted of a 24 mm objective lens (Nikon), mounted with a reversing ring on a 200 mm lens (Nikon). This combination yields a magnification of $200/24 = 8.3$ at f/1.7. To visualize suction flows, the water in the cuvette was seeded with monodisperse polystyrene spheres (10 μm in diameter; Phosphorex, Hopkinton, MA). The sample was illuminated from behind with a single LED (Luxeon Rebel, Lumiled, San Jose, CA). In this geometry, the silhouettes of individual particles were visible within the relatively transparent bladders and could be tracked manually to calculate fluid speed within the channel. The particle tracking procedure and analysis is described in greater detail in Berg O et al. (2020).

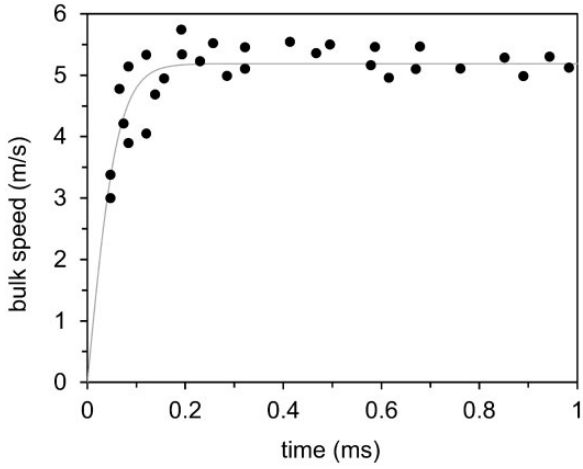

Fig. 3 Flow speed as observed by particle tracking in *U. gibba*. Points represent the maximum speed of individual particles, which occurs as they transit the point of minimum channel diameter (immediately downstream of the trap door). The solid line is a best fit of the data points to the unsteady inviscid Bernoulli equation, as given by Equation (9).

The results from these experiments (channel dimensions and flow speeds in the trap channel; Fig. 3) were used to develop the mechanical model described below (Berg et al. 2020).

Experiments using a mechanical model

Direct measurement on the plant samples is challenging due to the high spatial and temporal resolution required, and the degraded image quality within a bladder. Therefore, we constructed a mechanical model that can be dynamically scaled to reproduce the flow patterns characteristic of *U. gibba* (Fig. 1).

This model consists of a rigid housing of square cross-section, fitted with a square plunger. A computer-controlled linear actuator drives the plunger, which in turn drives fluid into and out of the housing through a relatively small test section mounted in its endplate. It is the flows within the test channel, and in the immediate vicinity of its entrance and exit, which are scaled to represent flows inside and outside the bladderwort.

Specifically, we consider the narrowest portion of the bladderwort channel, directly downstream of the trap door, where fluid speeds are the greatest. Our particle-tracking data at this location in actual bladders (Fig. 3) show that the maximum speed is $u_B = 5.2 \pm 0.2$ m/s, and the cumulative particle tracks indicate that this portion of the channel is typically $D_B = 96\,\mu$m in diameter by $L_B = 160\,\mu$m long (where subscript "B" is used to distinguish bladderwort from "M" for model; Berg et al. 2020). Together with the kinematic viscosity ν_B of water, the

characteristic Reynolds number of the internal suction flow is $Re = uL/\nu = 500$.

The test section of the mechanical model consists of a cylindrical channel $D_M = 32.0$ mm in diameter by $L_M = 53.0$ mm long. It operates in heavy mineral oil (CP200FG mineral oil; STE Oil Company, San Marcos, TX) of viscosity $\nu_M = 7.0 \times 10^{-5}$ m^2/s. When driven at a peak flow speed of $u_M = 1.09$ m/s, the desired $Re = 500$ is reproduced, and the flow field will be scaled accordingly. Distances in the model are thus scaled up by a factor of 320, and time duration is scaled up by a factor of 1470.

The test section is mounted coaxially in the base of the 191 mm × 191 mm square cross-section housing. Both are made of clear polycarbonate. This material is reasonably well index-matched to mineral oil, so internal flows are visible (except where the test section is bisected by the baseplate in which it is mounted). The fluid is driven by a polyethylene plunger fitted within the housing, which in turn is driven by an indexed solenoidal linear motor (LinMot, Lake Geneva, WI). Displacement of the plunger is programmed as a series of linear speed specifications and maintained by a Proportional–Integral–Derivative controller.

The model is not isomorphic with a bladder: the channel is idealized as a cylindrical tube, and the bladder as a square plunger. In common with real bladders, however, the surface that drives the flow has an area more than 100 × greater than the cross-sectional area of the channel. By continuity of flow, the resulting speeds (hence kinetic energies) are dominated by the immediate vicinity of the pipe entrance and exit. Because the driving pressure is applied between uniformly slow-moving fluid upstream and downstream of the test section, there is no distinction (in the idealized model) between the inside and outside of a bladder. Entry flows were generated by withdrawing the piston, and exit flows were generated by extending the piston. All physical surfaces were at least 2.5 gape diameters removed from the entrance or exit of the test section.

The mineral oil was seeded with air bubbles blown through a ceramic water filter. The bubbles were illuminated by a diode laser (Stocker-Yale/Coherent Lasiris Powerline, Salem, NH; 1500 mW at 810 nm) fitted with structured-light optics to form a sheet of uniform transverse intensity less than 1 mm thick throughout the field of view. Flow events were recorded with a Phantom V12.1 camera (Vision Research; Wayne, NJ) with the field of view 187 mm × 117 mm (Nikon 105 mm AF Micro Nikkor, f/2.8). With an effective sensitivity of 6400 ISO, 150 μs exposures produced non-saturated particle images with sub-pixel motion blur.

Particle image velocimetry PIV

The frame rate used for PIV analysis was 1000/s, with a real-world spatial resolution of 6.89 pixels/mm (1.47×10^6 frames/s scaled, at two 210 pixels/mm scaled). Cross-correlation vectors were obtained with the Mathworks MATLAB toolbox "PIVlab" (pre-processing: Contrast Limited Adaptive Histogram Equalization, window size 20 pixels; high-pass filter, kernel size 15 pixels; Wiener2 denoise filter, window size 3 pixels; PIV: FFT window deformation algorithm; two pass-PIV with interrogation area 64 pixels, step 32 pixels and interrogation area 32 pixels, step 16 pixels; Thielicke and Stamhuis 2014). Subsequent analysis and visualization of the vector fields were conducted in Mathematica (Wolfram Research).

Energy balance for fluid flow

In the following, we insert the previously described volume measurements on bladders and flow measurements on the mechanical model into an energy balance equation (mathematical model, Fig. 1). Both the evacuation of a bladder (which converts metabolic chemical energy into elastic potential energy) and a trapping event (which converts the elastic energy to kinetic energy of water) can be described as pumping processes. Since our experimental methods are adapted to measure flow properties, we monitor the energy budget by means of a balance over the moving fluid. With complete generality, the conservation of energy can be expressed as a rate balance between the change within an arbitrary volume $\mathcal{V}$ and the transport across its surface $\mathcal{S}$:

$$\frac{d}{dt}\{\text{energy within control volume } \mathcal{V}\} = -\frac{d}{dt}\{\text{energy crossing control surface } \mathcal{S}\} \quad (1)$$

We apply a macroscopic energy balance equation suitable for processes in which discrete streams enter and exit a volume of interest (such as a pump), and the density of the fluid is constant (Bird et al. 1960):

$$\frac{d}{dt}\left\{\left(U_{m_\nu} + \frac{u_\mathcal{V}^2}{2}\right) m_\nu\right\} = -\sum_i \left\{\left(U_{m_i} + \frac{u_{m_i}^2}{2} + p_i V_{m_i}\right) \frac{d}{dt} m_i\right\} + \dot{Q} - \dot{W}. \quad (2)$$

The mass $m_\mathcal{V}$ of enclosed fluid is represented by the left-hand expression, where it is multiplied by

the specific internal energy $U_{m_\mathcal{V}}$ to obtain the total internal energy $m_\mathcal{V} U_{m_\mathcal{V}}$, and multiplied by the square of fluid speed $u_\mathcal{V}^2$ to obtain the total kinetic energy $m_\mathcal{V} u_\mathcal{V}^2/2$. Because the flow is neutrally buoyant, all terms representing gravitational potential energy have been omitted. The summation on the right represents discrete, stationary entrance or exit channels where mass m_i crosses normal to the control surface $\mathcal{S}$ (with a velocity profile that is uniform or represented by a suitable average). In addition to internal and kinetic energy, pV energy can be transmitted by the fluid across $\mathcal{S}$, hence the term in which the mass flow of a given stream m_i is multiplied by the absolute pressure of that stream p_i and its specific volume V_{m_i}. $\dot{Q}$ and $\dot{W}$ represent energy crossing $\mathcal{S}$ by means other than transport of fluid (conventional heat and work). The latter includes expansion or contraction of the control volume itself, and "shaft" work not carried by the fluid. By engineering convention, flow of mass and work out of the control volume are positive in sign, but outward heat conduction is negative.

Energy expended to set the trap

To estimate the elastic energy required to set the trap, we quantify the volume of water inspired during the firing phase and assume that the inspired volume equals the net volume of water evacuated from the trap lumen while the trap is set. We consider a control volume that encloses the contents of the bladder lumen. The system is evacuated by ion channels over a period of hours; on this timescale, the process is isothermal and the kinetic energy is negligible. $\dot{W}$ includes the work of an incremental change of the control volume $d\mathcal{V}$ acting on the external pressure p_{ex}. A volume decrease also does work on the environment (the bladder itself) by deforming its walls: $\dot{W} = p_{ex} d\mathcal{V} + E_\mathcal{V} d\mathcal{V}$ (this notation, with volume-specific energy $E_\mathcal{V} < 0$, anticipates that elastic energy increases in proportion to evacuated volume). Considering the ion channels collectively as a single exit i, the differential energy balance (2) simplifies to

$$U_{m_\mathcal{V}} dm_\mathcal{V} = -U_{m_i} dm_i - p_i V_{m_i} dm_i - p_{ex} d\mathcal{V} - E_\mathcal{V} d\mathcal{V} + \dot{Q}. \quad (3)$$

The change of system mass is identical in magnitude to the expelled mass, so $dm_\mathcal{V} = -dm_i$, and the change of system volume is identical in magnitude to the expelled volume, so $d\mathcal{V} = -V_{m_i} dm_i$. Integrating over the loading process yields

$$\int E_\mathcal{V} d\mathcal{V} = \int (p_{in} - p_{ex}) d\mathcal{V} + (U_{m_\mathcal{V}} - U_{m_i}) \rho d\mathcal{V} + Q \quad (4)$$

where the density $\rho = 1/V_m$. This balance relates mechanical (elastic) energy stored outside the control volume, left, to fluid properties on the right.

A detailed model of the elastic behavior of the bladder, as developed by Joyeux et al. (2011), could specify the formal relationship between $E_\mathcal{V}$ and $(p_{in} - p_{ex})$ as a function of volume. In their finite-element simulation, neither the stored energy nor the pressure difference is simply related to each other or the bladder volume. Fortunately, direct manometric measurements of *Utricularia sp.*, *U. vulgaris* and *U. stellaris* during loading have shown that the internal pressure stabilizes early in the loading process, with more than 50% of water subsequently expelled against a constant pressure difference of 12–17 kPa (Sydenham and Findlay 1973; Sasago and Sibaoka 1985a; Singh et al. 2011). This pressure–volume characteristic is programmed by the elastic properties of the bladder walls and may be adapted for stability of the trigger mechanism across a range of loading states. With p_i and $E_\mathcal{V}$ independent of lumen volume, and the evacuation slow enough to be isothermal, the integration of Equation (4) is trivial.

$$E_\mathcal{V} \Delta\mathcal{V} = (p_{in} - p_{ex}) \Delta\mathcal{V} \quad (5)$$

In other words, the elastic energy stored is equal to the mechanical energy required to load the trap by expelling liquid.

Power expended during a suction event—estimate based on experimental flow fields

Because traps continue to evacuate lumen contents after they are ready to trigger, the degree of loading (hence total energy expended) is not entirely under experimental control. However, thanks to the aforementioned constancy of internal pressure and volume-specific elastic loading, the onset of a feeding strike, if not its duration, is expected to be uniform from trap to trap. Furthermore, the analysis of experimental velocity fields is simplified when the accelerated fluid is entirely within the control surface.

In order to apply the energy balance Equation (2) to flow fields from the scaled model, we construct a control surface that encloses a constant volume well removed from the high-speed flows at the entrance and exit of the test section. We furthermore idealize this distant flow field as crossing the control surface at uniform speed and normal incidence. These assumptions are borne out by examination of the measured flow fields during acceleration, but they

break down as the exit jet entrains fluid and approaches the edge of the video frame.

During the initial sub-millisecond acceleration, the kinetic energy of the fluid is not negligible, but the event is effectively adiabatic. Therefore, we retain kinetic energy terms in (2) but set $\dot{Q} = 0$. Neither the control volume nor the fluid mass that it contains changes in time ($d\mathcal{V}/dt = dm_\mathcal{V}/dt = 0$), and the mass flow rates of the input and output channels are equal in magnitude and opposite in sign ($dm_{\text{entrance}}/dt = -dm_{\text{exit}}/dt$). Using Δ to represent the difference between entrance and exit fluid properties, and $\dot{m}$ and $\dot{V}$ to represent the mass and volume flow rates, respectively,

$$m_v \frac{d}{dt} U_{m_v} + \frac{d}{dt}\left(\frac{m_v u^2}{2}\right) = -\Delta(U_{m_i} + p_i V_{m_i})\dot{m} \quad (6)$$

In this purely mechanical system, the internal energy of the fluid depends only on temperature. Viscous dissipation converts kinetic to internal energy on the left, and the rate at which it is transported out of the control volume appears on the right. A detailed accounting is beyond the scope of a macroscopic energy balance. We shall analyze model startup flows in control volumes that are operationally large; elements of the fluid that have experienced shear since the onset of flow do not cross the image boundary. Then a simplified power balance equates acceleration and temperature rise to the rate of potential energy loss:

$$\frac{d}{dt}\left(\frac{m_v u^2}{2}\right) + m_v \frac{d}{dt} U_{m_v} = -(p_{in} - p_{ex})\dot{V} \quad (7)$$

The kinetic energy change (left) can be obtained by integrating the kinetic energy function of an experimental velocity field at different times. Calculation of the potential energy change (right) requires measurements of bulk flow rate and pressure difference. An approximation for the latter is obtained by assuming that the pressure difference as a function of volume is simply the reverse of that observed during evacuation. This assumption is supported by its adequacy to explain the acceleration and terminal velocity of the jet as modeled by an unsteady Bernoulli equation. Previous particle-tracking data furthermore provide a measure of the bulk flow rate during early stages of the suction event (Berg et al. 2020).

The kinetic energy was obtained by first mapping the norms of the observed velocity vectors onto a scalar field of speeds, then creating a continuous scalar speed field $u(r, x)$ by linear interpolation. Assuming that the flow field is axisymmetric, its kinetic energy can be calculated by numerically integrating the kinetic energy function over a cylindrical polar volume element:

$$E_k = \int\int \frac{1}{2}\rho u^2 2\pi r \; dr \; dx \quad (8)$$

where x is longitudinal position along the axis of symmetry, r is radial distance from it, and ρ is the density of the fluid.

Results

Energy expended to set the trap

We measured the volume of water inspired during the firing phase in 15 traps of *U. gibba*. The inspired volume ranges from 0.01 to 0.04 µL (bladder length 0.8–1.2 mm; mean 1.0 ± 0.1 mm, $n = 15$) with a mean inspired volume of 0.016 ± 0.008 µL ($n = 15$); the range of values reflects variation in trap size and, more importantly, their loading state, with the latter depending on the time since the last suction event. In this context, we use the mean (0.016 µL) as well as the value that is most likely to represent a maximally loaded trap (0.040 µL). We assume a loading pressure of 15.0 kPa (Sydenham and Findlay 1973; Singh et al. 2011) based on values observed in other aquatic species, given that pressures are similar across species and not strongly correlated with trap size (Adamec and Poppinga 2016). This pressure yields a lower-limit estimate for the total energy required to maximally load a *U. gibba* trap: $(p_{\text{in}} - p_{\text{ex}})\Delta\mathcal{V} = (-15.0\text{kPa})(-0.04 \times 10^{-9}\ \text{m}^3) = 0.6\ \mu\text{J}$, which is stored in the bladder wall as elastic potential energy. The mean inspired volume yields an elastic energy of 0.2 ± 0.1 µJ. The metabolic energy required to do this mechanical work will be greater in so far as the process is not perfectly efficient.

Power released during the suction event

Our measurements of suction flow speeds in *U. gibba* can be used to estimate the potential energy expended during the early stages of a suction event. Measured flow speed data at the narrowest part of the channel (Fig. 3) were fit to a solution of the unsteady inviscid Bernoulli equation to yield (Berg et al. 2020):

$$u(t) = \left(5.2\frac{\text{m}}{\text{s}}\right)\tanh\left[\frac{5.2\frac{\text{m}}{\text{s}}}{2(0.00016\ \text{m})}t\right], \quad (9)$$

where 5.2 m/s is the terminal velocity (for a sustained pressure difference) and 0.16 mm is the observed channel length. In Fig. 3, this fit is shown as a solid line. To determine the power expenditure according

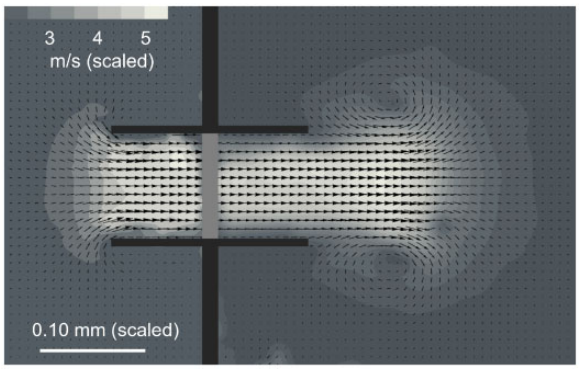

Fig. 4 Dynamically scaled model of fluid flow in *U. gibba*, in a plane containing the axis of cylindrical symmetry. Velocity vectors overlay an interpolated field of grayscale contours representing vector magnitude. The fluid is driven from left to right, through a cylindrical channel (cross section in black). Model parameters were chosen to reproduce $Re = 500$ as observed in *U. gibba*; the greatest speeds in this field are 5.7 m/s scaled (white). The entrance and exit flows were recorded separately at the same elapsed time since onset of flow, 0.10 ms (scaled). At this moment, the bulk acceleration of the fluid is complete.

to the right-hand side of Equation (7), we calculate the volume flowrate from the bulk linear flowrate and channel area (estimated based on gape, which is the diameter of the channel):

$$(p_{ex} - p_{in})\frac{d}{dt}\mathcal{V} = (p_{ex} - p_{in})\, u(t) \times \pi\left(\frac{\text{gape}}{2}\right)^2 \quad (10)$$

We have not attempted to correct for the development of the velocity profile. The flow is dominated by a uniform inviscid core, which is assumed to represent the bulk flow rate.

The power released according to Equation (10) appears in the fluid as internal energy (temperature rise) and kinetic energy. We evaluate the kinetic energy contribution by analysis of the model flow fields. A matching pair of experimental velocity flow fields (entrance and exit flow) is shown in Fig. 4. In Fig. 5, the separate contributions of the intake and exit flow are plotted as a function of time for the first 0.10 ms (scaled) of elapsed time since the onset of flow, the final points of which correspond to the flow fields in Fig. 4. Open circles in Fig. 5 show the sum of both contributions. The exit jet is first to develop, as the entire pressure head is acting to accelerate fluid along the channel. As the entry flow field develops, it consumes part of the pressure drop and exit-side acceleration. The sum evolves more slowly, and exhibits a maximum slope before the steady state is reached. The smooth curve is a logistic function, fit to the total kinetic energy data for the purpose of calculating the time derivative of total energy (power).

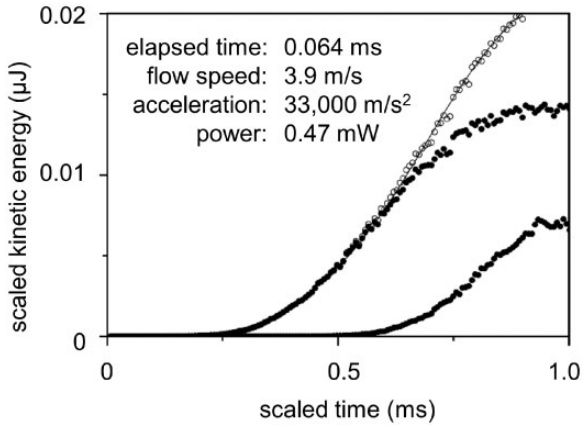

Fig. 5 Kinetic energy in the flow field of *U. gibba*, as determined from vector fields in the dynamically scaled model. The lower points represent each frame of the entrance flow field, which reaches a steady state at ~0.10 ms. The middle points represent the exit jet. The upper points (open symbols) show the total kinetic energy. The smooth curve is a fit of the logistic function to the total energy points. The slope of this curve measures the power appearing in the fluid in the form of kinetic energy. Listed are the conditions under which the scaled model is best matched to observations in bladderwort.

The mechanical model was driven by a constant-displacement program, not by constant pressure difference as in the plant. The program was tuned to reproduce the terminal speed (5.2 m/s) and the maximum acceleration (3.0×10^4 m/s^2) observed in particle-tracking measurements (Fig. 3). This acceleration was recorded 0.064 ms after the onset of flow—not because the acceleration is greatest at this time (Equation (9) predicts peak acceleration at the onset of flow), but because no tracer particles are present in the channel initially. Scaled values achieved in the model were 5.5 m/s and 3.3×10^4 m/s^2. Therefore, we perform the power balance at the elapsed time of maximum acceleration. Equation (10) yields 0.47 mW, while the time derivative of total energy in the scaled model is 0.46 mW. Therefore, the power balance between mechanical parameters measured on real bladders, and fluid flow measured in a dynamically scaled model, are in agreement: where the model is valid, roughly 0.5 mW is being converted.

Discussion

Low-loss suction flows

Given the approximations that have been used, the precision of agreement between the two terms of the power balance (elastic potential energy spent by bladderwort versus kinetic energy appearing in the mechanical model) is perhaps fortuitous. But the general agreement supports a picture of high-efficiency conversion of elastic potential energy to

kinetic energy of flow. Viscous dissipation, which would generate internal energy (heating) at the expense of kinetic energy in Equation (7), would appear in the current measurements as a discrepancy between potential and kinetic energy contributions to the observed power balance. To estimate the expected magnitude of frictional losses, we have calculated the frictional contribution to undeveloped steady-state flow (Langhaar 1942; Berg et al. 2020). Such conditions prevail in *U. gibba* strikes at times greater than 0.2 ms (Fig. 3). Using the same *U. gibba* parameters as elsewhere, the calculation predicts that 0.78 mW is expended at steady state, of which 17% (0.13 mW) is dissipated as friction within the channel. This magnitude of dissipation is below the experimental resolution of the current power balance. The driving pressure difference, in particular, is an approximation based on a small number of hydrostatic measurements in various bladderwort species. Furthermore, the presumed bulk flow rate observed in plants has not been adjusted in light of the detailed velocity profile (as observed for example in the scaled model, Fig. 4).

The observed flow field (Fig. 4) is characteristic of inviscid conditions. Its entrance and exit flows are different, with a steady-state sink pattern on the entrance side and an extending inertial jet (with vortex ring) on the exit side. Contours of constant speed are flat at the channel entrance, and their high spatial density indicates a steep pressure gradient directly in front of the channel mouth. The pressure-difference force in this region is believed to be the primary mechanism driving prey during suction feeding (Wainwright and Day 2007; van Wassenbergh and Aerts 2009b). At the exit, some development of a boundary layer is evident, but the flow is dominated by a uniform inviscid core. These properties are in accord with the modeled Reynolds number $Re = 500$, which is at the upper end of the intermediate flow regime ($1 < \mathrm{Re} < 1000$), in which discreet laminar boundary layers are present.

The conditions at the channel entrance are effective for the function of prey capture. They are created primarily by the large pressure difference between the inside and outside of the bladder. The pressure difference guarantees both a steep pressure gradient at the channel entrance, and a high uniform flow speed that is achieved early in the feeding strike.

Energy requirements for suction feeding in bladderworts

Bladderworts depend on elastic energy storage to power suction events. Plants power motion directly through hydraulic mechanisms or indirectly through elastic energy storage (Skotheim and Mahadevan 2005; Dumais and Forterre 2012). Hydraulic mechanisms severely limit speed, and the fastest plant movements are powered by elastic instability (Skotheim and Mahadevan 2005; Dumais and Forterre 2012). Bladderworts use a snap-buckle mechanism not only to operate the trap door (Joyeux et al. 2011; Vincent et al. 2011), but they also rely on elastically loading the walls of the traps to power the suction event (Joyeux et al. 2011).

Energy requirements for setting the trap can be calculated based on pressure–volume work (this study) or spring-deformation work (Joyeux et al. 2011). Using inspired water volume, we estimate that the elastic energy stored in the bladder walls of a fully loaded *U. gibba* trap (trap length 1 mm) is 0.6 μJ. A value of 11 μJ was reported for *U. inflata* (Joyeux et al. 2011). This bladderwort species is significantly larger both in total lumen volume and in fractional volume change during loading (Friday 1991), therefore more energy is spent evacuating lumen contents. The spring-deformation analysis of *U. inflata* is equivalent to a calculation of pressure–volume work, hence the stored-energy estimate is greater in direct proportion to the volume pumped (0.76 μL in *U. inflata* versus 0.040 μL in *U. gibba*).

Power requirements for small versus large suction feeders

Suction feeding requires considerable power to generate fast suction flows and steep pressure gradients. Adult fish (gape sizes 10–50 mm; van Wassenbergh et al. 2005; Higham et al. 2006b) generate suction pressures of 1–55 kPa (Carroll et al. 2004; van Wassenbergh et al. 2005), resulting in peak flow speeds in front of the mouth of 5–7 m/s (Higham et al. 2006b). Larval fish, with gapes below 0.5 mm, generate considerably weaker pressures of 0.2 kPa (Drost et al. 1988), resulting in weak suction flows of 0.001–0.003 m/s (Pekkan et al. 2016). Bladderwort stands out because they generate strong pressures (12–17 kPa; Sydenham and Findlay 1973; Singh et al. 2011) and strong suction flows despite their small size, reaching values similar to adult fish. The resulting mass-specific power for bladderwort (0.5 mW/0.16 mg = 3000 W/kg) is at the high end of values observed in suction-feeding fish (10–4000 W/kg; van Wassenbergh et al. 2005; Carroll and Wainwright 2009). Consistent with a scaling study in fish suction feeders, we find that small suction feeders face high power demands (van Wassenbergh et al. 2005). Bladderworts meet these

high power demands by storing considerable elastic energy over a long time period and then releasing this energy over an extraordinary brief time period.

The suction cycle of bladderworts is extremely asymmetric, with the loading phase taking many orders of magnitude longer than the firing phase. Bladderworts traps take typically 30 min to become ready to fire (Joyeux et al. 2011; Singh et al. 2011; Adamec and Poppinga 2016). The full resetting cycle lasts several hours ("6 to 10 hours": Adamec and Poppinga 2016; "several hours": Joyeux et al. 2011), and traps can remain loaded for days. In contrast, the firing phase is completed within a few milliseconds (Adamec and Poppinga 2016) from the trap being triggered to the prey being caught and the door closing. The main suction event is even shorter: the time to peak flow speed is well below 1 ms; in *U. gibba* it is roughly 0.1 ms (Fig. 4). With a loading period lasting 30 min to 10 h and an unloading period lasting 1 ms (0.1 ms for the time to peak flow), this yields a respectable ratio of unloading to loading duration of $1{:}10^7$ to $1{:}10^8$ ($1{:}10^8$ to $1{:}10^9$; Patek 2019). Bladderwort might not be unique in this extreme time asymmetry, as other plants also use elastic energy storage and explosive or snap-buckling unloading for prey capture and seed dispersal (review: Sakes et al. 2016; Galstyan and Hay 2018; Westermeier et al. 2018).

Acknowledgments

The photographs in Fig. 1 were taken by Mohammed Zaid Faizan Shaik. The mechanical model was developed in collaboration with Fatima Hidalgo.

Funding

This research was supported by the National Science Foundation [NSF-BIO-IOS #1352130 to U.K.M.] and California State University Fresno.

References

Adamec L, Poppinga S. 2016. Measurement of the critical negative pressure inside traps of aquatic carnivorous *Utricularia* species. Aquat Bot 133:10–6.

Aerts P, Osse J, Verraes W. 1987. Model of jaw depression during feeding in *Astatotilapia elegans* (Teleostei: Cichlidae): mechanisms for energy storage and triggering. J Morphol 194:85–109.

Berg O, Brown D, Schwaner MJ, Hall MR, Müller UK. Forthcoming 2020. Hydrodynamics of the bladderwort feeding strike. J Exp Zool A.

Bird R, Stewart WE, Lightfoot EN. 1960. Transport phenomena. Philadelphia (PA): John Wiley & Sons.

China V, Holzman R. 2014. Hydrodynamic starvation in first-feeding larval fishes. Proc Natl Acad Sci U S A 111:8083–8.

Camp AL, Roberts TJ, Brainerd EL. 2015. Swimming muscles power suction feeding in largemouth bass. Proc Natl Acad Sci U S A 112:8690–5.

Carroll AM, Wainwright PC, Huskey SH, Collar DC, Turingan RG. 2004. Morphology predicts suction feeding performance in centrarchid fishes. J Exp Biol 207:3873–81.

Carroll AM, Wainwright PC. 2006. Muscle function and power output during suction feeding in largemouth bass, *Micropterus salmoides*. Comp Biochem Physiol A Mol Integr Physiol 143:389–99.

Carroll AM, Wainwright PC. 2009. Energetic limitations on suction feeding performance in centrarchid fishes. J Exp Biol 212:3241–51.

D'amato P. 2013. The Savage Garden, revised: cultivating carnivorous plants. Berkeley, CA: Ten Speed Press.

Deban SM, Wake DB, Roth G. 1997. Salamander with a ballistic tongue. Nature 389:27.

Deban SM, Olson WM. 2002. Biomechanics: suction feeding by a tiny predatory tadpole. Nature 420:41.

Deban SM, O'Reilly JC, Dicke U, van Leeuwen JL. 2007. Extremely high-power tongue projection in plethodontid salamanders. J Exp Biol 210:655–67.

Drost MR, Muller M, Osse JWM. 1988. A quantitative hydrodynamical model of suction feeding in larval fishes: the role of frictional forces. Proc Biol Sci 234:263–81.

Dumais J, Forterre Y. 2012. "Vegetable dynamicks": the role of water in plant movements. Annu Rev Fluid Mech 44:453–78.

de Groot JH, van Leeuwen JL. 2004. Evidence for an elastic projection mechanism in the chameleon tongue. Proc Biol Sci 271:761–70.

Galstyan A, Hay A. 2018. Snap, crack and pop of explosive fruit. Curr Opin Genet Dev 51:31–6.

Friday LE. 1991. The size and shape of traps of *Utricularia vulgaris* L. Funct Ecol 5:602–7.

Higham TE, Day SW, Wainwright PC. 2006. The pressures of suction feeding: the relation between buccal pressure and induced fluid speed in centrarchid fishes. J Exp Biol 209:3281–7.

Higham TE, Day SW, Wainwright PC. 2006. Multidimensional analysis of suction feeding performance in fishes: fluid speed, acceleration, strike accuracy and the ingested volume of water. J Exp Biol 209:2713–25.

Holzman R, Day SW, Mehta RS, Wainwright PC. 2008. Jaw protrusion enhances forces exerted on prey by suction feeding fishes. J R Soc Interface 5:1445–57.

Holzman R, Collar DC, Mehta RS, Wainwright PC. 2012. An integrative modeling approach to elucidate suction-feeding performance. J Exp Biol 215:1–13.

Ilton M, Bhamla MS, Ma X, Cox SM, Fitchett LL, Kim Y, Koh J-S, Krishnamurthy D, Kuo C-Y, Temel FZ, et al. 2018. The principles of cascading power limits in small, fast biological and engineered systems. Science 360:eaao1082.

Joyeux M, Vincent O, Marmottant P. 2011. Mechanical model of the ultrafast underwater trap of *Utricularia*. Phys Rev E 83:021911.

Koehl M. 2003. Physical modelling in biomechanics. Philos Trans R Soc London B Biol Sci 358:1589–96.

Langhaar HL. 1942. Steady flow in the transition length of a straight tube. J Appl Mech 9:A55–A58.

Olberding JP, Deban SM. 2018. Scaling of work and power in a locomotor muscle of a frog. J Comp Physiol B 118:623–34.

Patek SN, Korff WL, Caldwell RL. 2004. Biomechanics: deadly strike mechanism of a mantis shrimp. Nature 428:819.

Patek SN. 2019. The power of mantis shrimp strikes: Interdisciplinary impacts of an extreme cascade of energy release. Integr Comp Biol (10.1093/icb/icz127).

Pekkan K, Chang B, Uslu F, Mani K, Chen CY, Holzman R. 2016. Characterization of zebrafish larvae suction feeding flow using μPIV and optical coherence tomography. Exp Fluids 57:112.

Poppinga S, Weisskopf C, Westermeier AS, Masselter T, Speck T. 2016. Fastest predators in the plant kingdom: functional morphology and biomechanics of suction traps found in the largest genus of carnivorous plants. AoB Plants 8:plv140.

Rutishauser R. 2016. Evolution of unusual morphologies in Lentibulariaceae (bladderworts and allies) and Podostemaceae (river-weeds): a pictorial report at the interface of developmental biology and morphological diversification. Ann Bot 117:811–32.

Sakes A, van der Wiel M, Henselmans PW, van Leeuwen JL, Dodou D, Breedveld P. 2016. Shooting mechanisms in nature: a systematic review. PLoS One 11:e0158277.

Sasago A, Sibaoka T. 1985a. Water extrusion in the trap bladders of *Utricularia vulgaris*. I. A possible pathway of water across the bladder wall. Bot Mag Tokyo 98:55–66.

Sasago A, Sibaoka T. 1985b. Water extrusion in the trap bladders of *Utricularia vulgaris*. II. A possible mechanism of water outflow. Bot Mag Tokyo 98:113–24.

Singh AK, Prabhakar S, Sane SP. 2011. The biomechanics of fast prey capture in aquatic bladderworts. Biol Lett 7:547–50.

Skotheim JM, Mahadevan L. 2005. Physical limits and design principles for plant and fungal movements. Science 308:1308–10.

Stinson CM, Deban SM. 2017. Functional trade-offs in the aquatic feeding performance of salamanders. Zoology (Jena) 125:69–78.

Sydenham PH, Findlay GP. 1973. The rapid movement of the bladder of *Utricularia* sp. Aust J Biol Sci 26:1115–26.

Thielicke W, Stamhuis E. 2014. PIVlab–towards user-friendly, affordable and accurate digital particle image velocimetry in MATLAB. J Open Res Software 2:e30.

Vincent O, Weisskopf C, Poppinga S, Masselter T, Speck T, Joyeux M, Quilliet C, Marmottant P. 2011. Ultra-fast underwater suction traps. Proc Biol Sci 278:2909–14.

Vincent O, Marmottant P. 2011. Carnivorous *Utricularia*: the buckling scenario. Plant Signal Behav 6:1752–4.

van Wassenbergh S, Aerts P, Herrel A. 2005. Scaling of suction-feeding kinematics and dynamics in the African catfish, *Clarias gariepinus*. J Exp Biol 208:2103–14.

van Wassenbergh S, Aerts P, Herrel A. 2006. Hydrodynamic modelling of aquatic suction performance and intra-oral pressures: limitations for comparative studies. J R Soc Interface 3:507–14.

van Wassenbergh S, Strother JA, Flammang BE, Ferry-Graham LA, Aerts P. 2008. Extremely fast prey capture is powered by elastic recoil. J R Soc Interface 5:285–96.

van Wassenbergh S, Aerts P. 2009. Rapid pivot feeding in pipefish: flow effects on prey and evaluation of simple dynamic modelling via computational fluid dynamics. J R Soc Interface 5:1291–301.

van Wassenbergh S, Aerts P. 2009. Aquatic suction feeding dynamics: insights from computational modelling. J R Soc Interface 6:149–58.

Wainwright PC, Kraklau DM, Bennett AF. 1991. Kinematics of tongue projection in *Chamaeleo oustaleti*. J Exp Biol 159:109–33.

Wainwright PC, Ferry-Graham LA, Waltzek TB, Carroll AM, Hulsey CD, Grubich JR. 2001. Evaluating the use of ram and suction during prey capture by cichlid fishes. J Exp Biol 204:3039–51.

Wainwright PC, Day SW. 2007. The forces exerted by aquatic suction feeders on their prey. J R Soc Interface 4:553–60.

Westermeier AS, Fleischmann A, Müller K, Schäferhoff B, Rubach C, Speck T, Poppinga S. 2017. Trap diversity and character evolution in carnivorous bladderworts (*Utricularia*, Lentibulariaceae). Sci Rep 7:12052.

Westermeier AS, Sachse R, Poppinga S, Vögele P, Adamec L, Speck T, Bischoff M. 2018. How the carnivorous waterwheel plant (*Aldrovanda vesiculosa*) snaps. Proc Biol Sci 285:20180012.

Yaniv S, Elad D, Holzman R. 2014. Suction feeding across fish life stages: flow dynamics from larvae to adults and implications for prey capture. J Exp Biol 217:3748–57.

Zack TI, Claverie T, Patek SN. 2009. Elastic energy storage in the mantis shrimp's fast predatory strike. J Exp Biol 212:4002–9.